

Low frequency radio observations of SN 2011dh and the evolution of its post-shock plasma properties

Naveen Yadav^{1,2*}, Alak Ray^{1,3†}, Sayan Chakraborti^{3,4‡}

¹Tata Institute of Fundamental Research, Homi Bhabha Road, Mumbai 400005, India

²Department of Physics, Indian Institute of Science, Bangalore 560012, India

³Institute for Theory and Computation, Harvard Smithsonian Center for Astrophysics, 60 Garden Street, Cambridge, MA 02138, USA

⁴Society of Fellows, Harvard University, 78 Mt. Auburn Street, Cambridge, MA 02138, USA

3rd March 2016

ABSTRACT

We present late time, low frequency observations of SN 2011dh made using the Giant Metre-wave Radio Telescope (GMRT). Our observations at 325 MHz, 610 MHz and 1280 MHz conducted between 93 – 421 days after the explosion supplement the millimeter and centimeter wave observations conducted between 4 – 15 days after explosion using the Combined Array for Research in Millimeter-wave Astronomy (CARMA) and extensive radio observations (1.0 – 36.5 GHz) conducted between 16 – 93 days after explosion using Jansky Very Large Array (JVLA). We fit a synchrotron self absorption model (SSA) to the 610 MHz and 1280 MHz radio light curves. We use it to determine the radius (R_p) and magnetic field (B_p) at 173 & 323 days after the explosion. A comparison of the peak radio luminosity L_{op} , with the product of the peak frequency ν_p and time to peak t_p shows that the supernova evolves between the epochs of CARMA, JVLA and GMRT observations. It shows a general slowing down of the expansion speed of the radio emitting region on a timescale of several hundred days during which the shock is propagating through a circumstellar medium set up by a wind with a constant mass loss parameter, \dot{M}/v_w . We derive the mass loss parameter (A_\star) based on 610 MHz and 1280 MHz radio light curves, which are found to be consistent with each other within error limits.

Key words: supernovae: individual (SN 2011dh) – stars: mass-loss – radiation mechanisms: non-thermal – radio continuum: general – techniques: interferometric.

1 INTRODUCTION

Identifying the nature of progenitors is a key question in the study of core-collapse and thermonuclear supernovae. Type IIb supernova are an intermediate class of core-collapse supernova between the Type II and Type Ib supernovae (Filippenko 1997). Their spectra show a transition from Type II supernovae (photospheric Balmer, H_α , lines in early time spectra, near maximum brightness) to a spectra characteristic of Type Ib supernovae (absence of broad H_α emission lines in late time spectra). The prototypical example of type IIb supernovae is SN 1993J. Their progenitor stars are believed to have lost most of the outer Hydrogen envelope prior to collapse. The mechanisms which can cause the star to lose their hydrogen envelope may differ for single stars vs stars in binaries. The binaries can have a) mass transfer with a companion star while b) stellar winds c) pulsations and eruptions of evolved supergiants can operate in both single and binary stars. Most models for the prototypical IIb SN 1993J were binary based (Nomoto et al. 1996,

1993; Ray et al. 1993; Podsiadlowski et al. 1993; Utrobin 1994; Woosley et al. 1994; Smith 2014). Therefore when the supernova is young the lines are formed in the thin Hydrogen envelope and as the supernova ejecta expands with age the inner and deeper layers are exposed revealing the Helium zone. Type IIb supernovae therefore provide a link between the progenitors of Hydrogen rich Type II (the Hydrogen envelope is intact before collapse) and Hydrogen poor Type Ib/c supernovae (massive stars stripped of their Hydrogen envelope). Chevalier & Soderberg 2010 have proposed that Type IIb supernovae can be sub-divided into compact IIb (Type cIIb) with $R_\star \sim 10^{11}$ cm) and extended IIb (Type eIIb) with $R_\star \sim 10^{13}$ cm) based on the mass-loss history and radius of the progenitor star and properties of the forward shock. Type eIIb have smooth radio light curves and slower shock, whereas Type cIIb have modulations in their radio light curves and high shock velocities ($\sim 0.1c$).

SN 2011dh is a Type IIb supernova which exploded in the spiral galaxy M51 (distance taken in this work $D \sim 8.4 \pm 0.6$ Mpc (Feldmeier et al. 1997)). It was discovered in the optical by A.Riou on 2011 May 31.89 UT; Griga et al. 2011 and on 2011 Jun 01.19 UT by the Palomar Transient Factory (PTF, Law et al. 2009; Rau

* naveen.phys@gmail.com

† akr@tifr.res.in

‡ schakraborti@fas.harvard.edu

et al. 2009); Silverman et al. 2011. Its evolution was followed in multiple wavelengths as it was a bright nearby supernova. Arcavi et al. 2011b suggested its classification as a Type IIb supernova on the basis of similarities between the spectrum of SN 2011dh reported by (Silverman et al. 2011) and a spectrum of SN 1993J and SN 2008ax.

In this work we present the Giant Metrewave Radio Telescope (GMRT) observations of SN 2011dh. We derive the properties of the post-shock plasma based on SSA model using combination of GMRT data and other archival data. We put together our results with published parameters based on Combined Array for Research in Millimeter-wave Astronomy (CARMA) and Jansky Very Large Array (JVLA, hereafter referred as VLA) data. In section 2, we present a brief summary of the published work on SN 2011dh and its progenitor star. In section 3 we present the radio observations and their reduction. The salient features of the radio emission model are discussed briefly in section 4. This is followed by the results in section 5. In section 6 we discuss the long term evolution of the parameters of this SN, including the long term mass loss from the progenitor before it exploded as obtained from CARMA, VLA and GMRT data.

2 PREVIOUS OPTICAL, RADIO AND X-RAY OBSERVATIONS OF SN 2011DH AND ITS PROGENITOR

SN 2011dh was discovered in radio by Horesh et al. 2011 on 2011 June 04.25 UT. Horesh et al. 2013 reported extensive early time (day 4 to day 16 after explosion) mm (33.6 GHz, 44.2 GHz, 93 GHz and 107 GHz) and cm (4.8 GHz, 5.0 GHz, 7.4 GHz, 8.5 GHz and 22.5 GHz) CARMA and VLA observations of SN 2011dh. They concluded that in order to reconcile the radio emission model (Chevalier 1998) and X-ray emission model (inverse Compton (IC) mechanism (Beall 1979; Chevalier 1982b)) an equipartition value¹, $f_{eB} \approx 500 - 1700$ is required, which leads to a shock wave velocity of $\sim 15000 \pm 1800 \text{ km s}^{-1}$. Soderberg et al. 2012 argued that the X-ray emission can be attributed to IC mechanism provided the equipartition assumption is relaxed ($f_{eB} \approx 30$ and $\epsilon_B \approx 0.01$) which leads to a doubling of mass loss rate. Krauss et al. 2012 observed radio emission (> 16 days) of SN 2011dh extensively with VLA and fitted the observations with the synchrotron self absorption model (Chevalier 1998). It is to be noted that there is a discrepancy in the shock velocity inferred by Soderberg et al. 2012 ($\sim 3.0 \times 10^9 \text{ cm/s}$) and Horesh et al. 2013 ($\sim 2.1 \times 10^9 \text{ cm/s}$) assuming equipartition. Maeda 2012 incorporated IC cooling to calculate the radio light curves and obtained strong constraints on the efficiency of the electron acceleration (ϵ_e) and magnetic field amplification (ϵ_B) in the post-shock region. They obtained $\epsilon_e < 0.01$, which is smaller by a factor of ~ 30 compared to the value suggested by Soderberg et al. 2012. Maeda 2012 also suggested that a single power law electron distribution cannot explain the radio and X-ray emission together and a pre-acceleration injection population of electrons peaking around Lorentz factor $\gamma \sim 20 - 30$ in addition to a power law extending to higher energy is required. It should be noted that the results of Horesh et al. 2013 and Soderberg et al. 2012 are based on early time (< 16 days) radio emission from SN 2011dh whereas the results of Krauss et al. 2012 are based on late time ($\sim 16 - 93$ days) radio emission.

¹ Equipartition factor (f_{eB}) is the ratio of fraction of post-shock energy density in relativistic electrons and post-shock magnetic field respectively.

Soderberg et al. 2012 inferred a high forward shock velocity $v_s \sim 0.1c$ on the basis of radio observations which indicated that the progenitor was compact. They also used the early time (< 5 days) optical observations to constrain the size of progenitor star. They found the progenitor star to be consistent with a compact progenitor at the time of explosion $R_* \sim 10^{11} \text{ cm}$ (Type cIIb) and is dissimilar from those of Type eIIb SNe. A similar conclusion was arrived at on the basis of the SN's optical light curve and measurement of its photospheric temperature Arcavi et al. 2011a. A putative progenitor was detected in the pre-explosion Hubble Space Telescope images by Li & Filippenko 2011, Maund et al. 2011 and Van Dyk et al. 2011. Maund et al. 2011 found that the progenitor star is consistent with an F8 supergiant star on the basis of its spectral energy distribution (SED). On the basis of comparison with stellar evolution tracks they suggested that it corresponds to a single star at the end of core C-burning with an initial mass of $M_{ZAMS} = 13 \pm 3 M_\odot$. Van Dyk et al. 2011 found that the star's radius ($\sim 10^{13} \text{ cm}$) is more extended than what has been inferred for the SN progenitor by Soderberg et al. 2012 and Arcavi et al. 2011a. They speculated that the detected star is either an unrelated star very near the position of the actual progenitor, or, more likely, the progenitor's companion in a mass-transfer binary system. They found the position of the detected star in a Hertzsprung-Russell (HR) diagram to be consistent with initial mass of $M_{ZAMS} \sim 17 - 19 M_\odot$. Murphy et al. 2011 estimated the mass of the progenitor based on stellar population synthesis and found that M_{ZAMS} to be in close agreement with the estimate of Maund et al. 2011. Early optical and near IR photometry and spectroscopy of SN 2011dh showed fast evolution. Ergon et al. 2014, 2015 found a small amount of hydrogen ($\sim 0.01 - 0.04 M_\odot$) in the envelope, and they made a detailed comparison with the prototypical type IIb SN 1993J.

Bersten et al. 2012 computed a set of hydrodynamical models and found that a large progenitor star with $R_* \sim 200 R_\odot$ is needed to reproduce the early light curve which was consistent with the hypothesis that the detected yellow-supergiant in the pre-explosion HST images was the progenitor star. They also suggested that a single star evolutionary scenario for the progenitor of SN 2011dh is unlikely. Benvenuto et al. 2013 proposed that the progenitor belongs to a close binary ($16 M_\odot + 10 M_\odot$) system on the basis of stellar evolutionary calculations following the evolution of both stars in the system. Van Dyk et al. 2013 reported the vanishing of yellow supergiant as seen in the pre explosion images which is consistent with the analysis by Bersten et al. 2012 and Benvenuto et al. 2013. There has been considerable debate about the nature of the residual emission from the location of the SN. Using HST observations in the F225W and F336W bands on day 1664, Folatelli et al. 2014 claimed that the residual blue point source was the hot compact companion of the progenitor YSG star that has exploded in 2011 as predicted by Benvenuto et al. 2013. This has however been contested by Maund et al. 2015 who argue on the basis of UV and optical HST observations at approximately the same day that the Spectral Energy Distribution (SED) of the late time source is inconsistent with that of a stellar source although a partial contribution to the observed UV flux from the possibly still present companion star cannot be ruled out. The separate claims of the two groups are subject to key assumptions made in their respective analyses. While Folatelli et al. 2014 assume that the UV flux originated only from the binary companion, Maund et al. 2015 show this is not borne out by the expected decrease of the flux at redder wavelengths and the observed SED is contrary to such expectations. On the other hand, the analysis of Maund et al. 2015 is subject to the assumption that there is no significant circumstellar interaction of the SN

which is contaminating the observed SED. Although they state that the presence of significant late time flux at optical wavelengths in SN 2011dh suggests that the UV flux is not necessarily attributable to a binary companion, a binary companion could still be hidden in the light of the SN itself thereby constraining the progenitor mass to a lower value than has been estimated so far. This in turn would imply that the mass transfer which stripped the progenitor star's hydrogen envelope was not very efficient (compared to the case for SN 1993J) and most of the mass lost from the progenitor may have been lost from the system rather than accreted on the companion. It is possible, as claimed by [Maund et al. 2015](#) that a binary companion is not a prerequisite for the progenitor of SN 2011dh, for e.g., SN 1993J which showed a significant evidence of a hot binary companion to its progenitor whereas in the case of SN 2008ax very late HST observations confirmed the disappearance of the original pre-supernova star and did not show any residual from a stellar remnant at the SN position. Our GMRT observations have bearing on these issues, which we describe below.

SN 2011dh was observed in X-rays using Swift from $\sim 3 - 50$ days after the explosion ([Margutti & Soderberg 2011](#); [Soderberg et al. 2012](#); [Campana & Immler 2012](#)). It was also observed by XMM-Newton on two epochs: 2011 June 07.20 UT & 2011 June 11.20 UT ([Campana & Immler 2012](#)) and by Chandra on two epochs : 2011 June 12.30 UT ([Pooley 2011](#)) & 2011 July 03.40 UT (PI: A.M. Soderberg) at early times. Chandra looked at M51 on 2012 Sept 09 through 2012 Oct 10 (PI: K.D. Kuntz), which provided a long exposure of SN 2011dh corresponding to 467 – 498 days after the explosion ([Maeda et al. 2014](#)). [Soderberg et al. 2012](#) reported spectral softening with time on the basis of spectrum extracted from June 3-7 (photon index: 0.9 ± 0.3) and June 7-17 (photon index: 1.8 ± 0.2) and also noted that the X-ray luminosity is lower by a factor of ≈ 10 compared to the well observed Type eIIB SN 1993J and SN 2001gd. According to their analysis, synchrotron emission at forward shock and free-free emission at reverse shock do not explain the the origin of X-ray emission. They suggested that the X-ray emission may be due to IC emission. [Sasaki & Ducci 2012](#) detected a hard component in the XMM-Newton spectrum taken at ~ 7 days which disappeared by ~ 11 days. They suggested that the soft component in the X-ray emission can be identified as IC emission while the harder component has its origin in the shocked circumstellar gas. [Campana & Immler 2012](#) have fitted the early time (7 day and 11 day) X-ray data with two hot diffuse gas component model originating at the forward shock and reverse shock respectively and also show the existence of a non-negligible absorption column in addition to Galactic column density. A similar study was done for the case of SN 1993J ([Uno et al. 2002](#)) in which it was found that the low-temperature component has much higher column depth than the high-temperature component. [Maeda et al. 2014](#) also derived mass-loss rate ($\sim 3 \times 10^{-6} M_{\odot} \text{ yr}^{-1}$ for wind velocity of $\sim 20 \text{ kms}^{-1}$) of the progenitor based on the late time (~ 500 days) Chandra X-ray observations. Note that X-rays and radio probe different parts of the SN with the reverse shock emission measure being sensitive to ejecta density profile, in addition to that of the circumstellar medium while the radio probes the blastwave shock's interaction with the CSM. The estimates of [Maeda et al. 2014](#) are based on very steep ($\rho_{\text{ej}} \propto r^{-n}$, $n \sim 20$) ejecta density profiles, which is similar to that inferred for SN 1993J ([Suzuki & Nomoto 1995](#); [Fransson et al. 1996](#)).

Table 1. Low frequency radio observations of SN 2011dh using GMRT (Giant Metrewave Radio Telescope). The Age is calculated assuming 2011 May 31.893 (MJD 55712.8) as the explosion date.

Date of Observation (UT)	Age (Days)	Frequency (GHz)	Flux (mJy)	Image RMS σ_1 (mJy)
2011-09-02	093	0.607	0.36	0.08
2011-10-20	141	0.607	1.27	0.09
2011-10-27	148	1.276	4.71	0.04
2011-10-31	152	0.323	<0.60	0.20
2012-01-15	228	0.323	1.17	0.19
2012-01-16	229	0.599	3.12	0.08
2012-01-16	229	1.277	5.90	0.03
2012-05-09	343	1.386	4.86	0.05
2012-05-16	350	0.608	4.53	0.09
2012-07-20	415	0.323	3.61	0.25
2012-07-21	416	0.607	4.24	0.07
2012-07-26	421	1.387	3.60	0.05

3 GMRT OBSERVATIONS AND DATA REDUCTION

The data presented in this work were acquired using the Giant Metrewave Radio Telescope (GMRT) in full intensity mode and with a 32 MHz bandwidth at 325 MHz, 610 MHz and 1280 MHz between 93–421 days after the explosion. Our observations supplement the millimeter (33.6 GHz, 44.2 GHz, 93 GHz and 107 GHz) and centimeter wave (4.8 GHz, 5.0 GHz, 7.4 GHz, 8.5 GHz and 22.5 GHz) observations conducted between 4 – 15 days after explosion using the CARMA and extensive radio observations (1.0 – 36.5 GHz) using the VLA conducted between 16 – 93 days after explosion. All the datasets have been analyzed using standard techniques in Astronomical Image Processing System (AIPS). Each dataset was manually flagged for instances of Radio Frequency Interference (RFI) and malfunctioning baselines and subsequently the raw visibilities were calibrated using 3C286 (which is both the flux calibrator as well as the phase calibrator). The bandpass calibrated dataset was used for imaging using the AIPS task IMAGR. The source flux was obtained using AIPS task JMFIT. The reported image RMS are obtained from the region surrounding the source. The details of the observation are presented in Table 1. The errors used in the analysis have been calculated using

$$\sigma_{\text{total}}^2 = \sigma_{\text{I}}^2 + \sigma_{\text{C}}^2, \quad (1)$$

to take in to account calibration errors and other unknown effects. Here σ_{I} is rms noise in the image and σ_{C} is the 10% of the determined flux taken as calibration error. The fitting results are summarized in Table 2.

4 SYNCHROTRON SELF ABSORPTION MODEL

Radio emission from core collapse supernovae has long been argued to be of non-thermal origin ([Chevalier 1982a,b](#); [Fransson & Björnsson 1998](#)). It originates at the forward shock where electrons are accelerated to relativistic energies and magnetic fields are strong. These electrons radiate by synchrotron mechanism in the post-shock amplified magnetic field. The early time, low frequency turnover in the spectral energy density seen in many SNe can be due to synchrotron self absorption (SSA) and/or free-free absorption (FFA) ([Chevalier 1982a, 1998](#)), and their relative importance in the context of the prototypical type IIB SN 1993J has been discussed by [Fransson & Björnsson 1998](#). We use the SSA model to fit our GMRT radio light curves and extract model parameters. [Krauss et al. 2012](#) also have used the SSA model to fit the early data

from VLA (and CARMA) of SN 2011dh. However, while [Krauss et al. 2012](#) fit the broad-band spectral energy distribution at specific epochs, we use the SSA model to fit our light curves.

We model the 610 MHz and the 1280 MHz data using the synchrotron self absorption model ([Chevalier 1998](#)). The electron index p (the electron energy distribution function index p is defined as: $N(E) \propto E^{-p}$) is taken to be 2.8 in accordance with [Krauss et al. 2012](#). The blast wave expands according to a power-law: $R \propto t^m$, where the value of m is taken to be: 0.87 ± 0.07 ([Krauss et al. 2012](#)). The non thermal radio flux at any given frequency can be written as ([Chevalier 1998](#))

$$\frac{F(t)}{F_{\text{op}}} = 1.582 \left(\frac{t}{t_p}\right)^a \left\{1 - \exp\left(-\frac{t}{t_p}\right)^{-(a+b)}\right\}, \quad (2)$$

where,

$$a = 2m + \frac{1}{2}; \quad b = \frac{p + 5 - 6m}{2}, \quad (3)$$

and where t_p is the age at which the optical depth becomes unity and F_{op} is the corresponding value of flux density. The values of radius (R_p) and post-shock magnetic field (B_p) are determined using the following formulas from [Chevalier 1998](#) (for $p = 2.8$ and $F_p = 1.5F_{\text{op}}$)

$$R_p = 4.1 \times 10^{14} f_{\text{eB}}^{-0.05} \left(\frac{f}{0.5}\right)^{-0.05} \left(\frac{F_{\text{op}}}{\text{mJy}}\right)^{0.47} \left(\frac{D}{\text{Mpc}}\right)^{0.95} \left(\frac{\nu}{5 \text{ GHz}}\right)^{-1} \text{ cm}, \quad (4)$$

$$B_p = 1.1 f_{\text{eB}}^{-0.21} \left(\frac{f}{0.5}\right)^{-0.21} \left(\frac{F_{\text{op}}}{\text{mJy}}\right)^{-0.10} \left(\frac{D}{\text{Mpc}}\right)^{-0.21} \left(\frac{\nu}{5 \text{ GHz}}\right) \text{ Gauss}, \quad (5)$$

where f is the fraction of supernova volume filled with synchrotron emitting plasma, D is the distance to the supernova and f_{eB} is the equipartition factor which is defined as:

$$f_{\text{eB}} = \frac{\epsilon_e}{\epsilon_B}, \quad (6)$$

where ϵ_e and ϵ_B are the fraction of energy density in relativistic electrons and post-shock magnetic field respectively. The wind density profile for the case of a constant mass loss rate \dot{M} , can be written as

$$\rho_w = \frac{\dot{M}}{4\pi v_w} r^{-2} = A r^{-2} \text{ g cm}^{-3}, \quad (7)$$

where v_w is the wind velocity. [Chevalier & Fransson 2006](#) redefine A in terms of A_\star as:

$$A_\star = \frac{A}{5 \times 10^{11} \text{ g cm}^{-1}}. \quad (8)$$

In the circumstellar interaction model a fraction ϵ_B , of the thermal energy of shocked medium is converted to post-shock magnetic field energy. The energy density in magnetic field u_B , can be related to the mass loss parameter A_\star , using Equation 8 from [Chevalier & Fransson 2006](#) as

$$u_B = \frac{B^2}{8\pi} = 0.052 \left(\frac{\epsilon_B}{0.1}\right) A_\star \left(\frac{t}{10 \text{ d}}\right)^{-2} \text{ erg cm}^{-3}. \quad (9)$$

The quantity A_\star can thus be related to the observed quantities by rewriting the above equation as

$$A_\star = 0.76 \left(\frac{\epsilon_B}{0.1}\right)^{-1} \left(\frac{t}{10 \text{ d}}\right)^2 B^2. \quad (10)$$

5 RESULTS

We fit the low frequency data with the synchrotron self absorption model (see Equation 2) which has been presented in the previous section (fixing the value of m and p from [Krauss et al. 2012](#)). The fits to the low frequency radio data are shown in Figure 1. The 610 MHz data point on 93.2 day falls on the spectrum reported by [Krauss et al. 2012](#) on 92.9 day as shown in Figure 3. The fit at 1280 MHz shown in Figure 1 (bottom panel) comprises of all the available L-Band data from GMRT and VLA ([Krauss et al. 2012](#)). The 1.40 GHz VLA data has been scaled to 1.28 GHz (using optically thick synchrotron emission scaling: $F_{1.28}/F_{1.40} = (1.28/1.40)^{5/2}$) for the purpose of fitting. We derive the values of R_p and B_p using Equation 4 & 5 and assuming equipartition ($f_{\text{eB}} = 1$).

We can use the radio emission models derived by ([Krauss et al. 2012](#)) and [Horesh et al. 2013](#) to predict the radio flux densities for GMRT observations. We have plotted the predicted flux densities based on model from [Krauss et al. 2012](#) and [Horesh et al. 2013](#) along with the observed flux densities in Figure 1 & 2. [Krauss et al. 2012](#) have used the SSA model to fit the broadband radio spectra on various days. The model is written as (Equation 1 in [Krauss et al. 2012](#))

$$S(\nu) = 1.582 S_{\nu_\tau} \left(\frac{\nu}{\nu_\tau}\right)^{5/2} \left\{1 - \exp\left[-\left(\frac{\nu}{\nu_\tau}\right)^{-(p+4)/2}\right]\right\}, \quad (11)$$

where S_{ν_τ} is the flux density at frequency ν_τ , at which the optical depth is unity. The [Krauss et al. 2012](#) predictions shown in Figure 1 & 2 are calculated using their fit parameters for broadband radio spectra at 92.9 day ($S_{\nu_\tau} = 6.44 \pm 0.21$ mJy and $\nu_\tau = 2.235 \pm 0.076$ GHz). We have taken the parameters corresponding to 92.9 day as it is the closest to GMRT observation epoch on 93 day and onwards. To calculate the flux densities based on [Horesh et al. 2013](#) we have used the following equations from [Horesh et al. 2013](#):

$$S = K1 \left(\frac{\nu}{5 \text{ GHz}}\right)^\alpha \left(\frac{t - t_0}{1 \text{ day}}\right)^\beta \left(\frac{1 - e^{-\tau_{\text{ssa}}}}{\tau_{\text{ssa}}}\right), \quad (12)$$

$$\tau_{\text{ssa}} = K5 \left(\frac{\nu}{5 \text{ GHz}}\right)^{\alpha-2.5} \left(\frac{t - t_0}{1 \text{ day}}\right)^{\delta''}, \quad (13)$$

where $K1$ and $K5$ are proportionality constants and δ'' describes the time dependence of the optical depth (the parameters have the values $\alpha = -1.15$, $\beta = -0.96$, $K1 = 453.43$, $K5 = 1.9772 \times 10^5$ & $\delta'' = -3.42$, with 1σ errors of 6, 8, 8, 12 and 3%, respectively.). We find that the predicted flux densities from [Horesh et al. 2013](#) deviate more from the observed late time data compared to the predicted flux densities based on the model from [Krauss et al. 2012](#). This may be due to the fact that the two models were based on different time ranges of observations and the parameters that determine the radio emission have changed with time. This is in contrast to many cases where the radio emission from a supernova can be consistently fitted with a model valid across temporal and frequency coverage of the observations. We note that [Fransson & Björnsson 1998](#) advocated an evolution in the shock speed for the case of SN 1993J, with a break after ~ 100 days. For the case of 325 MHz observations, we have detection at two epochs and an upper limit on the flux density. Therefore we have not attempted to fit the radio light curve, and we show the observed data in Figure 2 along with the predicted values. We have obtained radius and magnetic field at two epochs using Equation 4 & 5. The errors in these

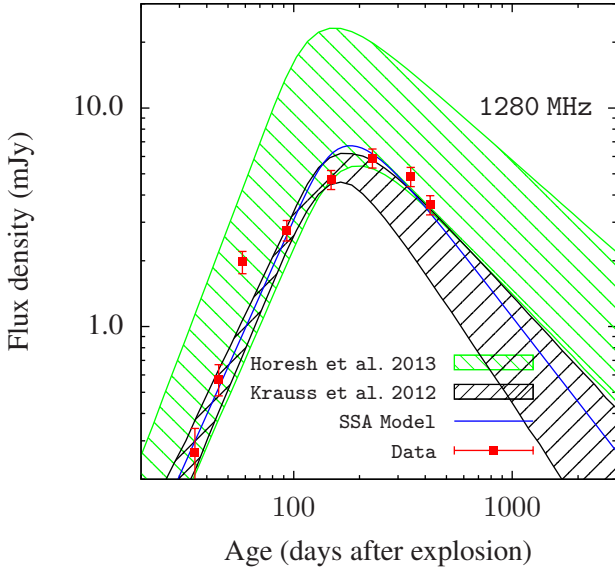
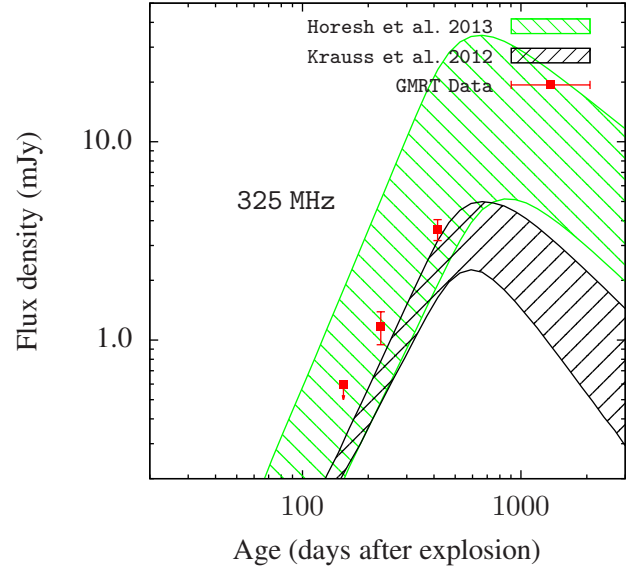
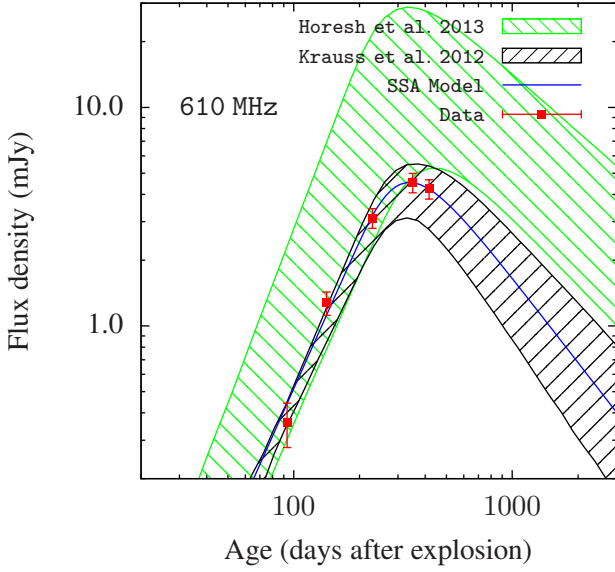


Figure 2. The 325 MHz data of SN 2011dh. The green and black shaded regions are predictions of the 310 MHz fluxes made using the model and parameters reported in Horesh et al. 2013 and Krauss et al. 2012 respectively.

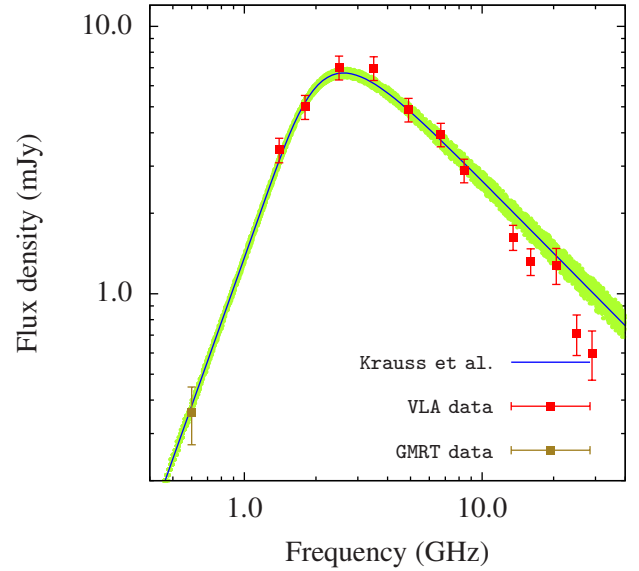


Figure 1. The 610 MHz data (upper panel) and 1280 MHz data (lower panel) of SN 2011dh fitted with the synchrotron self absorption model (see section 4) (Chevalier 1998). The curve at 1280 MHz consists of GMRT and VLA data (Krauss et al. 2012) (Here, 1.4 GHz flux is scaled to 1.28 GHz using optically thick scaling: $F \propto \nu^{5/2}$). The best fit parameters for the fits are reported in the Table 2. The green and black shaded regions are predictions of the 610 MHz & 1280 MHz fluxes made using the model and parameters reported in Horesh et al. 2013 ($\alpha = -1.15$, $\beta = -0.96$, $K1 = 453.43$, $K5 = 1.9772 \times 10^5$ & $\delta'' = -3.42$, with 1σ errors of 6, 8, 8, 12 and 3%) and Krauss et al. 2012 (at 92.9 day, $S_{\nu_r} = 6.44 \pm 0.21$ mJy and $\nu_r = 2.235 \pm 0.076$ GHz) respectively.

Figure 3. The 610 MHz GMRT data point at 93.2 day plotted along side the spectrum on 92.9 day reported by Krauss et al. 2012. The solid curve is the best fit to the spectrum as reported by Krauss et al. 2012 and it shows that 610 MHz flux density determined by GMRT is consistent with the SSA model fitted only to the VLA data on 92.9 day. The green shaded region corresponds to the uncertainties in the fit parameters.

Table 2. Results of the fit to low frequency GMRT radio observations of SN 2011dh. The Age is calculated assuming 2011 May 31.8 UT as the explosion date. The value of ϵ_B is taken to be 0.1 in calculating A_\star .

Frequency	1280 MHz	607 MHz
Peak flux density (mJy)	6.20 ± 0.16	4.51 ± 0.23
Age at peak (days)	173.6 ± 11.9	323.1 ± 11.3
Radius (10^{16} cm)	2.79 ± 0.23	4.89 ± 0.35
Magnetic field (Gauss)	0.135 ± 0.003	0.069 ± 0.001
A_\star	4.4 ± 0.60	3.72 ± 0.29
χ^2_ν	4.8	0.8

quantities have been estimated using

$$\frac{\delta R_p}{R_p} = \left(\left(0.47 \frac{\delta F_{op}}{F_{op}} \right)^2 + \left(0.95 \frac{\delta D}{D} \right)^2 + \left(\frac{\delta v_p}{v_p} \right)^2 \right)^{1/2}, \quad (14)$$

$$\frac{\delta B_p}{B_p} = \left(\left(0.10 \frac{\delta F_{op}}{F_{op}} \right)^2 + \left(0.21 \frac{\delta D}{D} \right)^2 + \left(\frac{\delta v_p}{v_p} \right)^2 \right)^{1/2}. \quad (15)$$

In Figure 4, we plot the radius and magnetic field values we obtain along with the values reported in literature (Krauss et al. 2012; Horesh et al. 2013; Bietenholz et al. 2012; de Witt et al. 2016) for the purpose of comparison. Our GMRT measurements taken along with VLA and Very long Baseline Interferometry (VLBI) measurements are consistent with a deceleration index $m = 0.96$ for radio sphere evolution. The values of dimensionless parameter A_\star (using $\epsilon_B = 0.1$) are plotted in Figure 5. All the points are based on fitting a radio spectra except the latest two points, which are based on 610 MHz and 1280 MHz (VLA+GMRT) light curves, therefore the corresponding A_\star is valid for the entire duration of the corresponding light curve at a given frequency. There are small variations in the mass loss rate ($\dot{M} = 6.2 \times 10^{12} v_w A_\star \text{ gm s}^{-1}$), but the average value of A_\star is around $\sim 3.7^{+1.3}_{-0.3}$. Using this $A_\star = 3.7$ we obtain a nearly constant value of mass loss rate of, $\dot{M} = 7.2 \times 10^{-7} M_\odot \text{ yr}^{-1}$ for a yellow supergiant progenitor with an assumed wind speed of $v_w = 20 \text{ km/s}$. In Figure 6, we plot F_{op} vs. $v_p t_p$ using all the fits from Horesh et al. 2013 and Krauss et al. 2012 including our measurements based on 610 MHz and 1280 MHz. This type of plot was used by Chevalier 1998 to distinguish between different types of supernovae on the basis of their radio emission properties. The peak luminosity L_{op} and mean forward shock velocity v_p can be related (for $p = 2.8$) using Equation 4 as

$$v_p = 3.6 \times 10^9 f_{eB}^{-0.05} \left(\frac{f}{0.5} \right)^{-0.05} \left(\frac{L_{op}}{10^{26} \text{ erg s}^{-1} \text{ Hz}^{-1}} \right)^{0.47} \left(\frac{v}{5 \text{ GHz}} \right)^{-1} \left(\frac{t_p}{10 \text{ days}} \right)^{-1} \text{ cm s}^{-1}, \quad (16)$$

where $L_{op} = 4\pi D^2 F_{op}$ is the peak radio spectral luminosity. We can use it to make lines for various values of v_p on a $L_{op} - v_p t_p$ plot which are shown in Figure 6. We note that object moves on the plot between various constant velocity lines and the velocity decreases as the object ages. The average shock velocity $2.5 \times 10^9 \text{ cm s}^{-1}$ (based on $f_{eB} = 1$) quoted by Krauss et al. 2012 appears to be on the left corner of this diagram (refer to Figure 6), while that of the Horesh et al. 2013 overlaps with the range of velocities shown between the black and blue lines. The shock appears to slow down with time according to this diagram which supports $m < 1$.

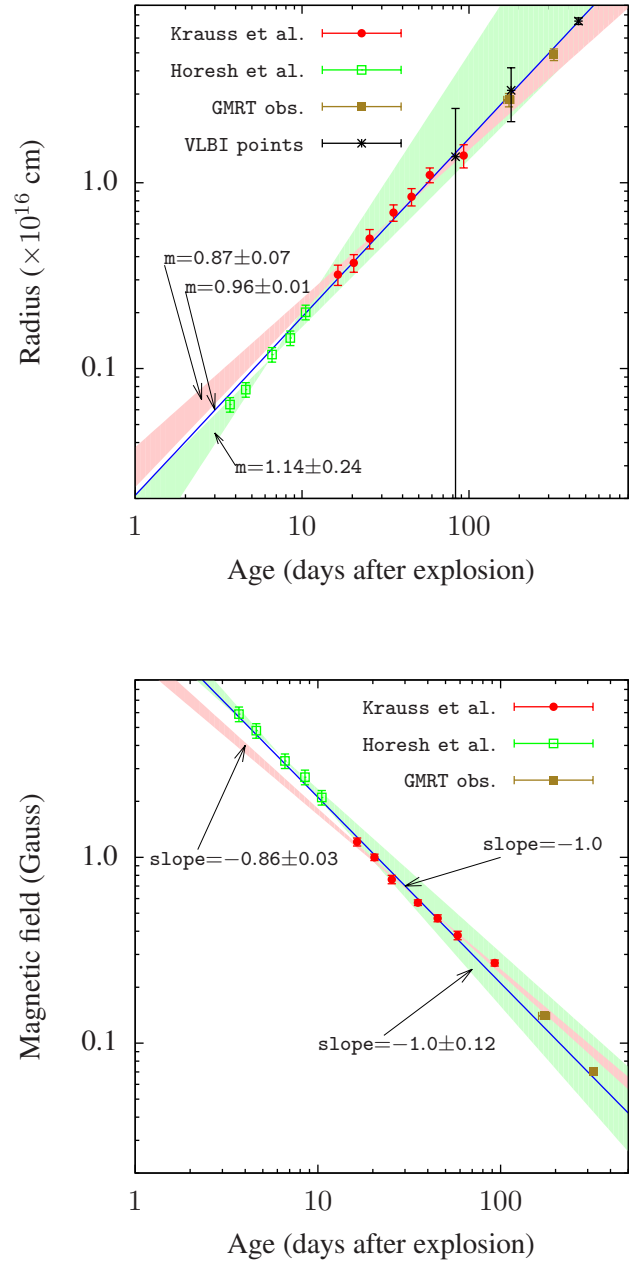


Figure 4. The radius (upper panel) and magnetic field (lower panel) at the two epochs determined using low frequency data presented along with the values obtained by Horesh et al. 2013 using CARMA, Krauss et al. 2012 using VLA and by Bietenholz et al. 2012; de Witt et al. 2016 using Very Large Baseline Interferometry (VLBI) data. The shaded red area corresponds to lines with $m = 0.87 \pm 0.07$ obtained by Krauss et al. 2012, while the shades green area with $m = 1.14 \pm 0.24$ correspond to the early radio data as obtained by Horesh et al. 2013 and the line with $m = 0.96 \pm 0.01$ is based on value reported in de Witt et al. 2016.

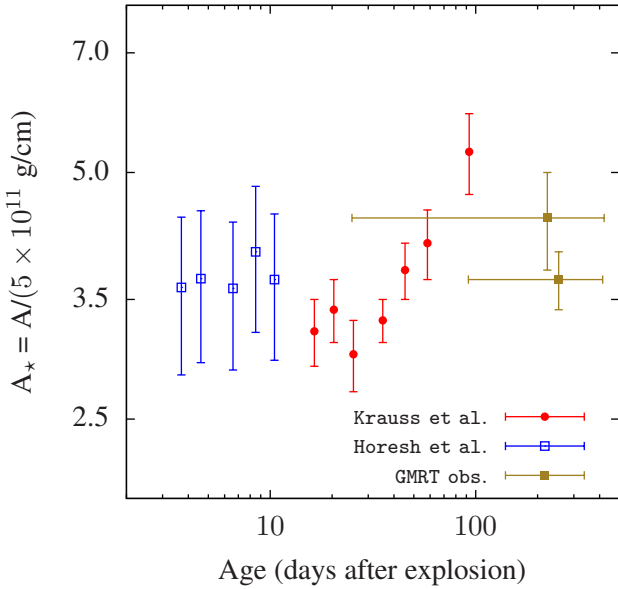


Figure 5. The mass loss parameter A_* plotted for the observation time range of 3 – 450 days. The parameter shows some variation which is consistent with an average value of around 3.5. All the points are calculated based on $\epsilon_B = 0.1$ and are based on fitting a radio spectra except the last two points, which are based on 610 MHz and 1280 MHz (VLA+GMRT) light curve. The corresponding A_* is therefore valid for the entire duration of the respective light curve.

6 DISCUSSIONS

In Figure 4 we show the time evolution of the shock wave radius based on GMRT data together with VLBI and early VLA data. We have drawn a line with slope $m \sim 0.96$ (de Witt et al. 2016), and the shaded error regions correspond to error in the fits by Krauss et al. 2012 ($m \sim 0.87 \pm 0.07$) and Horesh et al. 2013 ($m \sim 1.14 \pm 0.24$). It is evident that the SN shock has been propagating through a circumstellar medium set up by a wind with constant mass loss parameter, \dot{M}/v_w . If we assume that a pre-SN stellar wind speed, $v_w = 20$ km/s (corresponding to the constant wind speed of a yellow supergiant), then the radio observations imply an average value of mass loss rate of $\dot{M} = 7.2 \times 10^{-7} M_\odot \text{yr}^{-1}$, which is a factor of ~ 4 smaller than the determination by Maeda et al. 2014 from X-ray analysis. We note that the deviations of predicted flux densities from the observed radio flux densities is more for the case of Horesh et al. 2013 compared to Krauss et al. 2012 (see Figure 1 & 2). Horesh et al. 2013 found a value of m which is marginally consistent with the physically acceptable m obtained by Krauss et al. 2012, ($m \sim 0.87 \pm 0.07$) and the former authors' central value of index m was biased on the higher side of unity which is in an improbable dynamical regime given the asymptotic solution due to Chevalier 1982a for a shock wave in medium set up by a wind with constant mass loss rate, has the shock decelerating as $m = (n - 3)/(n - 2) < 1$, where n is the index for ejecta density profile. A possible reason may be the change in the properties of the blast wave or the electron population with time as the Horesh et al. 2013 model is based on very early time data while Krauss et al. 2012 model is based on slightly late time data. It is noted

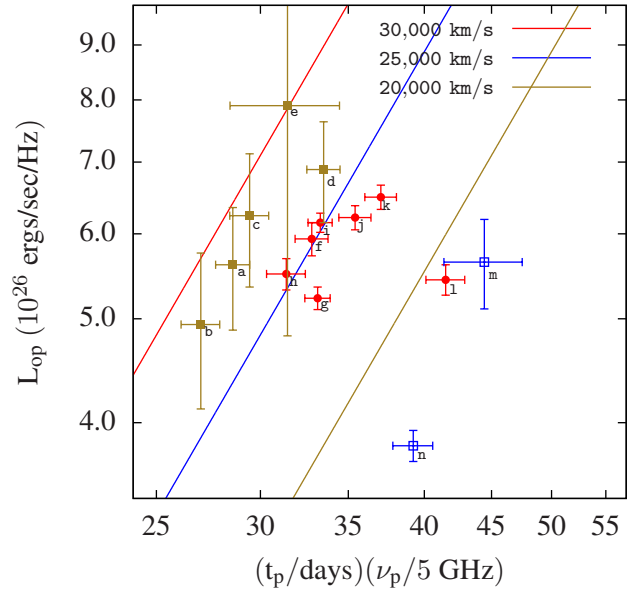


Figure 6. The $L_{op} - v_p t_p$ plot for SN 2011dh showing all the points obtained using the fits reported by Horesh et al. 2013 (filled squares), Krauss et al. 2012 (filled circles) and the values obtained using low frequency late time data (empty squares). The points labeled as [a, b, c, d, e, f, g, h, i, j, k, l, m & n] correspond to [3.7, 4.6, 6.6, 8.5, 10.5, 16.4, 20.4, 25.4, 35.3, 45.3, 58.2, 92.9, 173.6 & 323.1] days respectively. The constant velocity lines have been obtained using Equation 16 as in Chevalier 1998. Note the evolution between expansion speeds at early times (VLA) to late times (GMRT).

that the velocity of blastwave seems to have decreased with time as expected for an interacting blast wave (shown in Figure 6). The points are located between constant velocity lines corresponding to $2.5 \times 10^9 \text{ cm s}^{-1}$ and $3.0 \times 10^9 \text{ cm s}^{-1}$ at early time (< 58 days), and thereafter (> 90 days) move towards lower values of velocity of around $2.0 \times 10^9 \text{ cm s}^{-1}$. On the basis of early optical spectra Arcavi et al. 2011a suggested that the supernovae had a compact progenitor ($R_* \sim 10^{11} \text{ cm}$). Soderberg et al. 2012 also supported the hypothesis with a compact progenitor star using the initial X-ray and radio data. On the other hand, a slowed down shock as found in the size estimates of the radio sphere based on synchrotron spectra from early CARMA, VLA and our late time GMRT data is consistent with a type eIIB classification (Chevalier & Soderberg 2010). Also, the VLBI measurements of de Witt et al. 2016 confirms that by 453 days, the average expansion velocity was reduced to $1.89 \pm 0.28 \times 10^9 \text{ cm s}^{-1}$ (modulo a slightly different smaller distance of ~ 7.8 Mpc). Also, type cIIB SNe show late time radio variability as for example in SN 2001ig (Ryder et al. 2004) or SN 2003bg (Soderberg et al. 2006) which SN 2011dh did not display. The fact that the GMRT radio data is also consistent with evolution from the earlier VLA phase (albeit a shock speed change between 58 to 92 days) points to the extended nature of type progenitor rather than a compact Wolf-Rayet progenitor.

The residual blue point source found at the location of SN 2011dh could be due to a combination of the following four possible causes as pointed out by Maund et al. 2015, namely: a) a binary companion of the exploded supernova YSG progenitor, b) light echo from dust around the SN position, c) SN 2011dh itself (either

due to Freeze-out in the Helium envelope or in combination with radioactivity powered optical emission) and d) due to circumstellar interaction of the SN. [Maund et al. 2015](#) discard the light echo scenario (case-b) due to the special arrangement of dust directly behind the SN in the line of sight required to produce the point-like residual source. They also use their Swift X-ray Telescope (XRT) and VLA observations to argue against ongoing CSM interaction at the time of late time HST observations. However, we note that their 5 ksec XRT exposure gives a 3σ upper limit of 1.2×10^{39} erg s⁻¹ which is higher than the predicted X-ray luminosity (5×10^{37} erg s⁻¹ at 500 days). ([Soderberg et al. 2012](#)) based on early Swift data and the measured Chandra luminosity of 5.5×10^{37} erg s⁻¹ which is much lower even at 500 days ([Maeda et al. 2014](#)) i.e. half the age of the SN considered by [Maund et al. 2015](#). Therefore the X-ray observations do not rule out any ongoing strong CSM interaction continuing till 1164 days as claimed by [Maund et al. 2015](#). They further claim that their VLA observation on October 18, 2014 UT (day 1236) which showed a radio flux density of 459 ± 93 μ Jy in the C-band (6.1 GHz) and 109 ± 17 μ Jy in the K-band (22 GHz) are well within the expectations based on earlier VLA measurements, assuming that the CSM has an extended wind-like structure. As already argued here, the [Horesh et al. 2013](#) predictions somewhat overestimate the optically thin part of the emission in the L-band even during our GMRT observation epochs. In fact, with our GMRT L-band (1.387 GHz) measurements on day 421, we would expect about 230 μ Jy at 6.1 GHz and on day 1229 using Equation 12 & 13 which is about half of what has been reported. This, together with the evidence of early slowing down of the shock both in our GMRT data as well as in the long term average of VLBI measurements show that there is fairly strong ongoing CSM interaction which may have even been enhanced by day 1229 and must be contributing substantially in other bands (optical and UV included) within the as yet point source. There is also evidence that the nebular line profiles of SN 2011dh observed between 201 and 678 days show a roughly spherical explosion with a few aspherical clumps and the SN is showing signs of strong CSM interaction ([Shivvers et al. 2013](#)). However, the CSM interaction may decrease with time if the circumstellar wind is roughly spherically symmetric and with time may even be resolved if it continues to remain strong.

A comparison with the prototypical type IIb SN 1993J which had a considerable fraction of its hydrogen envelope stripped off prior to explosion shows that SN 2011dh had less radio luminosity at its peak and it evolved much more rapidly compared to SN 1993J (see [de Witt et al. 2016](#) for a comparison). This fast rise to peak of the radio light curve as well as the low peak luminosity imply that the CSM surrounding SN 2011dh was less dense than that for SN 1993J. There is thus variation of the properties of the environment and past history of the progenitors of the same spectroscopic type of SN.

7 CONCLUSIONS

We find that the radio emission models based on early time data (< 16 days) of SN 2011dh are not very suitable for predicting the late time (> 100 days) radio flux densities. This may be because the parameters of the shock-CSM interaction may have varied over time as exemplified by e.g. the variation of shock wave velocity with time. Such a hypothesis will be the scope of future investigations in similar types of SNe. We note that the SN 2011dh has many unsettled questions regarding binarity, mass and mass loss of

the progenitor which if probed will go a long way in helping us understand supernovae and their progenitors in general.

8 ACKNOWLEDGMENTS

We wish to acknowledge the support of TIFR 12th Five Year Plan (Project No: 12P-0261). NY wishes to thank Asaf Horesh for his valuable comments on the manuscript. NY wishes to acknowledge the support of CSIR-SPM fellowship (SPM-07/858(0057)/2009-EMR-I). AR thanks the director and staff of ITC, Harvard University for their hospitality during his leave of absence from TIFR. We thank the staff of the GMRT who have made these observations possible. GMRT is run by the National Centre for Radio Astrophysics of the Tata Institute of Fundamental Research.

References

- Arcavi I., et al., 2011a, *ApJ*, **742**, L18
 Arcavi I., et al., 2011b, *The Astronomer's Telegram*, **3413**, 1
 Beall J. H., 1979, *ApJ*, **230**, 713
 Benvenuto O. G., Bersten M. C., Nomoto K., 2013, *ApJ*, **762**, 74
 Bersten M. C., et al., 2012, *ApJ*, **757**, 31
 Bietenholz M. F., Brunthaler A., Soderberg A. M., Krauss M., Zauderer B., Bartel N., Chomiuk L., Rupen M. P., 2012, *ApJ*, **751**, 125
 Campana S., Immler S., 2012, *MNRAS*, **427**, L70
 Chevalier R. A., 1982a, *ApJ*, **258**, 790
 Chevalier R. A., 1982b, *ApJ*, **259**, 302
 Chevalier R. A., 1998, *ApJ*, **499**, 810
 Chevalier R. A., Fransson C., 2006, *ApJ*, **651**, 381
 Chevalier R. A., Soderberg A. M., 2010, *ApJ*, **711**, L40
 Ergon M., et al., 2014, *A&A*, **562**, A17
 Ergon M., et al., 2015, *A&A*, **580**, A142
 Feldmeier J. J., Ciardullo R., Jacoby G. H., 1997, *ApJ*, **479**, 231
 Filippenko A. V., 1997, *ARA&A*, **35**, 309
 Folatelli G., et al., 2014, *ApJ*, **793**, L22
 Fransson C., Björnsson C.-I., 1998, *ApJ*, **509**, 861
 Fransson C., Lundqvist P., Chevalier R. A., 1996, *ApJ*, **461**, 993
 Griga T., et al., 2011, *Central Bureau Electronic Telegrams*, **2736**, 1
 Horesh A., et al., 2011, *The Astronomer's Telegram*, **3411**, 1
 Horesh A., et al., 2013, *MNRAS*, **436**, 1258
 Krauss M. I., et al., 2012, *ApJ*, **750**, L40
 Law N. M., et al., 2009, *PASP*, **121**, 1395
 Li W., Filippenko A. V., 2011, *The Astronomer's Telegram*, **3399**, 1
 Maeda K., 2012, *ApJ*, **758**, 81
 Maeda K., Katsuda S., Bamba A., Terada Y., Fukazawa Y., 2014, *ApJ*, **785**, 95
 Margutti R., Soderberg A., 2011, *The Astronomer's Telegram*, **3420**, 1
 Maund J. R., et al., 2011, *ApJ*, **739**, L37
 Maund J. R., et al., 2015, *MNRAS*, **454**, 2580
 Murphy J. W., Jennings Z. G., Williams B., Dalcanton J. J., Dolphin A. E., 2011, *ApJ*, **742**, L4
 Nomoto K., Suzuki T., Shigeyama T., Kumagai S., Yamaoka H., Saio H., 1993, *Nature*, **364**, 507
 Nomoto K., Iwamoto K., Suzuki T., Pols O. R., Yamaoka H., Hashimoto M., Hoflich P., van den Heuvel E. P. J., 1996, in van Paradijs J., van den Heuvel E. P. J., Kuulkers E., eds, *IAU Symposium Vol. 165, Compact Stars in Binaries*. p. 119
 Podsiadlowski P., Hsu J. J. L., Joss P. C., Ross R. R., 1993, *Nature*, **364**, 509
 Pooley D., 2011, *The Astronomer's Telegram*, **3456**, 1
 Rau A., et al., 2009, *PASP*, **121**, 1334
 Ray A., Singh K. P., Sutaria F. K., 1993, *Journal of Astrophysics and Astronomy*, **14**, 53
 Ryder S. D., Sadler E. M., Subrahmanyam R., Weiler K. W., Panagia N., Stockdale C., 2004, *MNRAS*, **349**, 1093
 Sasaki M., Ducci L., 2012, *A&A*, **546**, A80

- Shivvers I., et al., 2013, *MNRAS*, **436**, 3614
- Silverman J. M., Filippenko A. V., Cenko S. B., 2011, The Astronomer's Telegram, **3398**, 1
- Smith N., 2014, *ARA&A*, **52**, 487
- Soderberg A. M., Chevalier R. A., Kulkarni S. R., Frail D. A., 2006, *ApJ*, **651**, 1005
- Soderberg A. M., et al., 2012, *ApJ*, **752**, 78
- Suzuki T., Nomoto K., 1995, *ApJ*, **455**, 658
- Uno S., et al., 2002, *ApJ*, **565**, 419
- Utrobin V., 1994, *A&A*, **281**, L89
- Van Dyk S. D., et al., 2011, *ApJ*, **741**, L28
- Van Dyk S. D., et al., 2013, *ApJ*, **772**, L32
- Woosley S. E., Eastman R. G., Weaver T. A., Pinto P. A., 1994, *ApJ*, **429**, 300
- de Witt A., Bietenholz M. F., Kamble A., Soderberg A. M., Brunthaler A., Zauderer B., Bartel N., Rupen M. P., 2016, *MNRAS*, **455**, 511